Water Resources Research

TECHNICAL REPORTS: METHODS
10.1029/2019WR025699

Bias Correction of Airborne Thermal Infrared Observations Over Forests Using Melting Snow

Steven Pestana[1], C. Chris Chickadel[2], Adrian Harpold[3], Tihomir S. Kostadinov[4,5], Henry Pai[6,7], Scott Tyler[8], Clare Webster[9,10], and Jessica D. Lundquist[1]

[1]Department of Civil and Environmental Engineering, University of Washington, Seattle, WA, USA, [2]Applied Physics Laboratory, University of Washington, Seattle, WA, USA, [3]Department of Natural Resources and Environmental Science, University of Nevada, Reno, Reno, NV, USA, [4]Department of Liberal Studies, California State University San Marcos, San Marcos, CA, USA, [5]Previously at Division of Hydrologic Sciences, Desert Research Institute, Reno, NV, USA, [6]Northwest River Forecast Center, National Weather Service, NOAA, Portland, OR, USA, [7]Peviously at Department of Geological Sciences and Engineering, University of Nevada, Reno, Reno, NV, USA, [8]Department of Geological Sciences and Engineering, University of Nevada, Reno, Reno, NV, USA, [9]WSL Swiss Federal Institute for Snow and Avalanche Research SLF, Davos, Switzerland, [10]School of GeoSciences, University of Edinburgh, Edinburgh, UK

Key Points:
- Thermal infrared camera bias was reduced by using the surface temperature of melting snow as a reference target
- Retrieval of the surface temperature variability of forests and snow was found to depend on the spatial distribution of forest stands
- Off-nadir observations over forests hindered snow surface temperature retrievals, but enabled improved canopy temperature measurements

Supporting Information:
- Supporting Information S1

Correspondence to:
S. Pestana,
spestana@uw.edu

Citation:
Pestana, S., Chickadel, C. C., Harpold, A., Kostadinov, T. S., Pai, H., Tyler, S., et al. (2019). Bias correction of airborne thermal infrared observations over forests using melting snow. *Water Resources Research*, *55*, 11,331–11,343. https://doi.org/10.1029/2019WR025699

Received 2 JUN 2019
Accepted 26 NOV 2019
Accepted article online 11 DEC 2019
Published online 12 DEC 2019

Abstract Uncooled thermal infrared (TIR) imagers, commonly used on aircraft and small unmanned aircraft systems (UAS, "drones"), can provide high-resolution surface temperature maps, but their accuracy is dependent on reliable calibration sources. A novel method for correcting surface temperature observations made by uncooled TIR imagers uses observations over melting snow, which provides a constant 0 °C reference temperature. This bias correction method is applied to remotely sensed surface temperature observations of forests and snow over two mountain study sites: Laret, Davos, Switzerland (27 March 2017) in the Alps, and Sagehen Creek, California, USA (21 April 2017) in the Sierra Nevada. Surface temperature retrieval errors that arise from temperature-induced instrument bias, differences in image resolution, retrieval of mixed pixels, and variable view angles were evaluated for these forest snow scenes. Applying the melting snow-based bias correction decreased the root-mean-square error by about 1 °C for retrieving snow, water, and forest canopy temperatures from airborne TIR observations. The influence of mixed pixels on surface temperature retrievals over forest snow scenes was found to depend on image resolution and the spatial distribution of forest stands. Airborne observations over the forests at Sagehen showed that near the edges of TIR images, at more than 20° from nadir, the snow surface within forest gaps smaller than 10 m was obscured by the surrounding trees. These off-nadir views, with fewer mixed pixels, could allow more accurate airborne and satellite-based observations of canopy surface temperatures.

1. Introduction

Thermal infrared (TIR) remote sensing can provide spatially distributed surface temperature measurements of forests and snow in the mountains where in situ measurements are sparse and model representation of the spatial and temporal heterogeneities of snow cover is difficult (Nolin, 2011). Spatially resolved measurements of snow surface temperature (T_{ss}) can help evaluate snow surface energy balance model performance (Lapo et al., 2015), while measurements of forest canopy temperature (T_f) provide information about the downward longwave radiation emitted onto the snow below (Webster et al., 2017). Forest canopy temperatures, serving as a proxy for air temperatures (Howard & Stull, 2013), can also provide information about lapse rates and cold air pooling over mountain terrain (Lundquist & Cayan, 2007; Whiteman, 2004).

The relatively low cost of both uncooled TIR cameras and small unmanned aircraft systems (UAS) has allowed more researchers to use airborne TIR observations for measurements of stream temperature (Cristea & Burges, 2009; Pai et al., 2017), soil moisture (Wigmore et al., 2019), geothermal activity (Harvey et al., 2016), in precision agriculture (Ribeiro-Gomes et al., 2017), and as validation data for testing remote sensing downscaling methods (Lundquist et al., 2018; Yang et al., 2016). However, methods to constrain the errors associated with airborne TIR instruments, including bias, are needed to improve the accuracy of surface temperature retrievals for these applications. Furthermore, the effects on surface temperature retrievals over forests and snow from off-nadir view angles and mixed pixels, where the spectral radiance

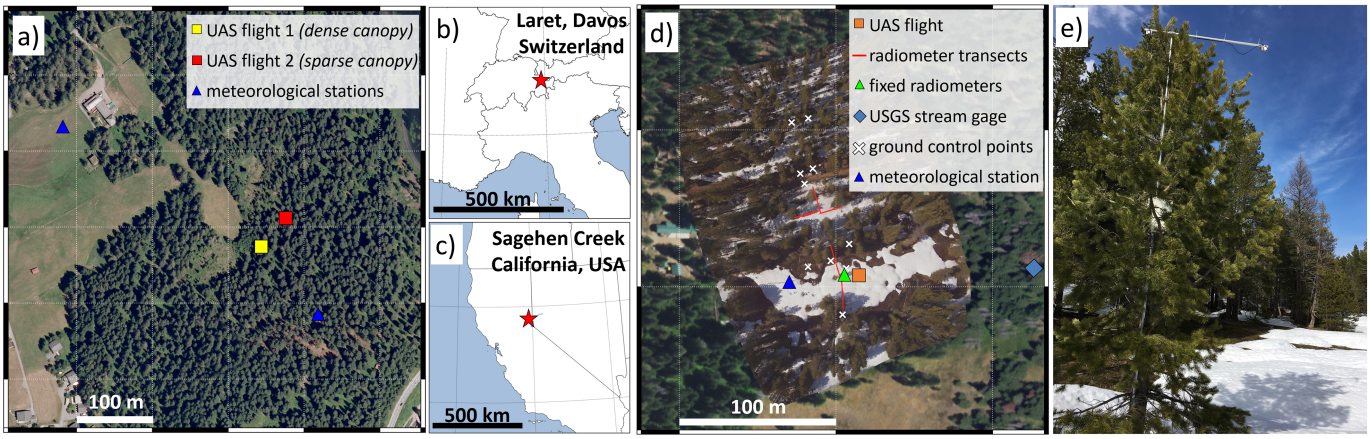

Figure 1. Study sites include (a) Laret, Davos on 27 March 2017 (b) in the Alps of eastern Switzerland and (c) in the Sierra Nevada of California, USA, (d) Sagehen Creek Field Station on 21 April 2017. (e) IR radiometers measuring the surface temperature of a conifer tree canopy, and the adjacent open snow surface at Sagehen Creek. (Background imagery: [a] Copernicus, ESA, 3 October 2009, Davos, Switzerland, 46.85°N, 9.88°E, Google Satellite TMS; and [d] National Agriculture Imagery Program, USDA FSA, 12 July 2016.)

from surfaces of different temperatures contribute to the total radiance sensed by a single pixel, need better characterization. This is particularly important for airborne observations that are relied on as a source of fine spatial resolution ground truth for model evaluation or comparison with space-based remote sensing.

This project capitalizes on the uniform temperature of melting snow (0 °C) and uses airborne TIR observations from various altitudes in two forest snow environments to answer the following questions:

1. What are the magnitudes of errors in TIR observations of forest snow environments caused by instrument bias?
2. How representative are the airborne TIR measurements of the true surface temperatures at varying spatial scales?
3. How do image resolution, mixed pixels, and off-nadir view angles contribute to surface temperature retrieval biases over forests and snow?

2. Study Sites, Data, and Instruments

2.1. Study Sites and In Situ Observations

Surface temperature observations were made at the Laret, Davos, study site in eastern Switzerland (46.845° N, 9.872°E) on 27 March 2017 (13:58–14:15 CEST). This site is situated within the subalpine forests of the Swiss Alps, about 6 km northeast of the city of Davos (Figure 1a) and at an elevation of 1,520 m. This forested site consists largely of Norwegian spruce (*Picea abies*) and some European larch (*Larix decidua*) trees, with heights of 20–40 m (Webster et al., 2018). Two meteorological stations provided in situ measurements of T_{ss} from infrared (IR) radiometers throughout the day, one measuring in an open area and the other beneath the forest canopy.

Sagehen Creek Field Station (39.432°N, 120.239°W) is located at an elevation of 1,950 m within the Tahoe National Forest in the eastern Sierra Nevada of California, USA, about 40 km north of Lake Tahoe (Figure 1d). Field observations of surface temperatures were made at Sagehen on 21 April 2017. The surrounding forest consists largely of lodgepole pines (*Pinus contorta*) and Jeffrey pines (*Pinus jeffreyi*), with average tree heights of 30 m. In situ measurements of T_{ss} and T_f, were made by a pair of boom-mounted Apogee SI-111 IR radiometers (Figure 1e and Figure S2a in the supporting information) viewing open snow surface and a tree canopy, respectively. Apogee IR radiometer measurements along a series of 20 m transects provided information about T_{ss} across the study site (Figure S4c). Water temperature (T_w) data for Sagehen Creek from a nearby USGS stream gage (Figure S3b) was accessed through the USGS National Water Information System (USGS, 2016; Figure 1d).

Table 1
Aircraft, Fights and TIR Instrument Specifications

	Sagehen Creek Field Station California, USA			Laret, Davos, Switzerland
Aircraft	Cessna 172 *(UW APL)*		Tarot 650 Sport UAS w/Pixhawk Flight Controller *(AirCTEMPs)*	DJI S1000 UAS *(Northumbria University)*
Flight date and times (local times)	21 April 2017 13:16–13:52		21 April 2017 15:15–15:25	27 March 2017 1) 13:58–14:01 2) 14:13–14:15
Flight altitudes AGL	1,000 m		20–70 m	40–110 m
TIR Instrument	DRS UC640-17	KT15.85D	ICI 8640P	Optris PI450
Total number of images (subset used for analysis)	1,018 (84)	—	112 (41)	1) 112 (70) 2) 143 (70)
Detector size	640 × 480	—	640 × 512	382 × 288
Pixel pitch	17 μm	—	17 μm	25 μm
Detector sensitivity (NEΔT)	0.07 °C	0.02 °C	0.02 °C	0.04 °C
Mfr. stated accuracy	—	±0.5 °C	±1.0 °C	±2.0 °C
Spectral range	8–14 μm	9.6–11.5 μm	7–14 μm	7.5–13 μm
Focal length	15.5 mm (f/1.1)	—	12.5 mm	15 mm
Field of view	40° × 30°	1.9°	50° × 37.5°	38° × 29°
Spatial resolution	1.0–2.0 m	35 m spot size	0.03–0.10 m	0.07–0.20 m

2.2. Airborne Observations

At the Davos site, a DJI S1000 multirotor UAS (system described within Webster et al., 2018) recorded airborne TIR imagery (Optris PI450 TIR camera) from altitudes of 40–110 m above ground level (AGL; Figure S2c). Two flights were conducted centered over tree canopies within forest stands of different canopy densities. Individual TIR images from these flights are used in the analysis of the effects of decreasing image resolution over snow and forest scenes on observed surface temperatures.

A TIR system (with DRS UC640-17 TIR camera and KT15.85D radiometer) developed by the University of Washington Applied Physics Laboratory (APL) was mounted on a Cessna 172 aircraft (system described within Lundquist et al., 2018) and made observations of the Sagehen site from an altitude of 1000 m AGL (13:16–13:52 PST; Figure S2a). A Tarot 650 multirotor UAS (Pai et al., 2016) made finer resolution TIR observations (ICI 8640P TIR camera) over the Sagehen site, from altitudes of 20–70 m AGL (15:15–15:25 PST; Figure S2b). The UAS TIR images are used in the analysis of image resolution over snow and forest scenes. The TIR images from the APL aircraft are used to demonstrate the effects of image resolution and off-nadir view angles on retrieving surface temperatures over forest snow environments. The bias correction method presented in this work is tested on individual images from these two different platforms over the melting snow at Sagehen.

2.3. TIR Imagers

The TIR imagers used in this study (Table 1; Figure S2) contain uncooled microbolometer arrays, sensitive to a range of wavelengths in the thermal infrared described by a spectral response function (Budzier & Gerlach, 2011). In response to the temperature of objects within each microbolometer sensor element's instantaneous field of view, they experience a change in the net radiation within this spectral range. This causes each sensor element to change temperature as it receives or emits a spectral radiance (W sr^{-1} m^{-2} μm^{-1}). As microbolometers change temperature, their resistance changes, which is measured and recorded as an electrical signal. TIR imagers are calibrated to relate these electrical signals to a corresponding temperature, given an estimation of the observed surface's emissivity. Emissivity describes how the radiance of a surface compares to the radiance of a blackbody (a perfect emitter) at the same kinetic temperature. The brightness temperature of an object within an image scene can be calculated from this radiance through inverting the Planck equation, whereas an object's emissivity must be included to calculate its kinetic temperature (Norman & Becker, 1995).

Without active thermal regulation to maintain a constant sensor temperature, varying camera body temperature (due to changing ambient air temperature, incident sunlight, or self-heating from electrical components, especially shortly after turning on a TIR camera) can result in biases in retrieved surface temperatures (Dugdale et al., 2019; Shea & Jamieson, 2011). In order to make accurate observations of absolute, rather than relative, surface temperatures consistently across a series of images, periodic recalibrations are required to adapt to changing ambient conditions.

Typically, as in the case of the two UAS-mounted TIR cameras, an internal shutter is closed over the sensor array at regular intervals. This provides a reference for the camera body temperature, which is used to update the camera calibration, as well as for a nonuniformity correction to adjust for differences in individual pixel responses to a uniform scene (e.g., vignetting; Abolt et al., 2018; Kelly et al., 2019; Ribeiro-Gomes et al., 2017). However, this method can only provide recalibrations as frequent as the shutter is closed and, unless the shutter is mounted externally, does not account for thermal radiation emitted by the lens (typical TIR camera shutters shut between the lens and microbolometer array). Alternatively, calibrated surface temperatures observed with a higher accuracy instrument could be used to vicariously calibrate TIR images in a postprocessing method. This vicarious technique (Text S1), was employed with the aircraft's TIR system for observations over Sagehen, which also included a nonuniformity correction to correct for vignetting effects.

Prior studies using uncooled TIR imagers on UAS have relied on internal shutters (Webster et al., 2018), performed laboratory calibrations with blackbody targets and measured internal camera temperatures (Nugent et al., 2013), or used blackbody-like calibration targets-of-opportunity with high emissivities during the data collection flights, such as glacial ice (Kraaijenbrink et al., 2018) or water (Baker et al., 2019; Harvey et al., 2016). Independently measuring the surface temperatures of calibration targets in the field allows for TIR images to be calibrated in postprocessing, where images containing the targets can be adjusted to match the independent target temperature measurements (Aubry-Wake et al., 2015; Wigmore et al., 2019), and images without the target in view can be adjusted to match overlapping images that do contain the targets (Gómez-Candón et al., 2016; Sheng et al., 2010).

Setting up calibration targets in the field requires additional resources and can be difficult or impossible in remote or hazardous locations, such as snow-covered mountain forests, or glaciers. Repeat imaging of targets by an airborne TIR sensor in a single flight are also needed to provide periodic calibration updates due to rapidly changing TIR camera temperature. This requirement constrains the spatial extent that can be covered, especially with the short flight times of battery-dependent small UAS. In cases where not every image contains a target, a functional form of the bias, such as linear drift as a function of time must then be assumed for bias corrections in between calibration images (Jensen et al., 2014; Mesas-Carrascosa et al., 2018). Using the melting snow surface as a natural, near-blackbody, target-of-opportunity allows images to be individually corrected for bias without having to develop a bias model, or place field targets over large areas, enabling large surveys over snow-covered areas.

3. Methods

3.1. TIR Bias Correction

To quantify and correct for instrument bias in uncooled TIR imagers, we developed and tested a novel bias correction method using the melting snow surface as a natural radiometric calibration target. Ground-based radiometer measurements of the snow surface temperature at Sagehen show it maintained a constant 0 °C throughout the day (Figure S4), as it was actively melting under clear sky conditions with near-surface air temperatures reaching a daily maximum of 16 °C. Snow surface temperature measurements along four transects showed snow melting whether in direct sunlight or shaded by canopies.

The emissivity of melting snow in the thermal infrared is around 0.99, and largely insensitive to differences in snow grain size, or view angles less than 20° (Dozier & Warren, 1982; Warren, 1982). This makes melting snow very close to an ideal blackbody target. The TIR cameras and radiometers used in this study measured brightness temperature, with an assumed scene emissivity of 1. The difference between brightness temperature and true surface temperatures for melting snow (Lundquist et al., 2018) and conifer trees (Salisbury & D'Aria, 1992) is minimal in comparison with TIR imager bias and other potential sources of error (see Text S2).

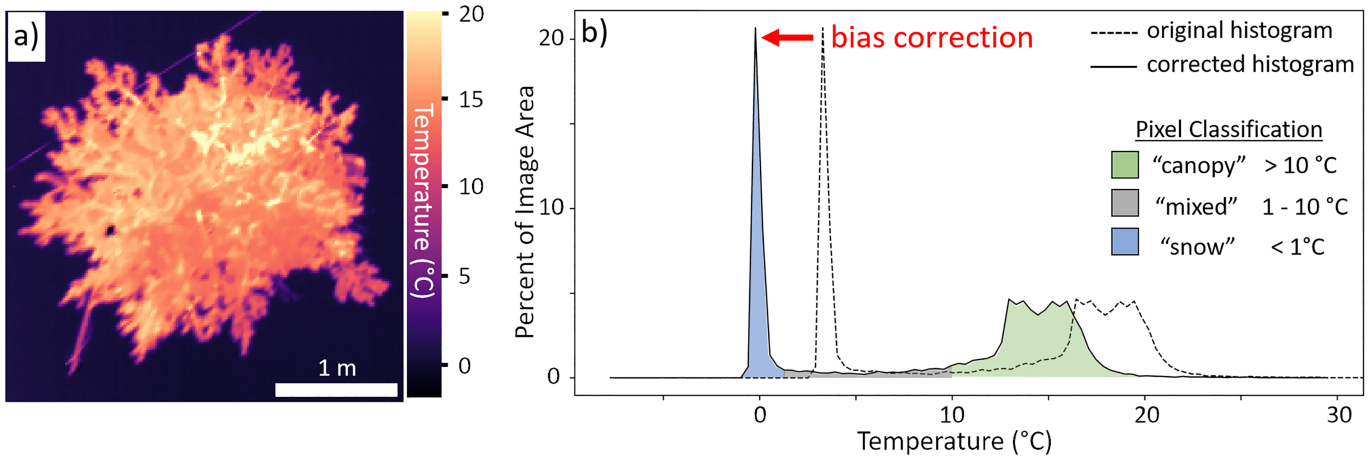

Figure 2. (a) TIR image from the UAS directly over the instrumented tree at Sagehen and (b) its corresponding histogram before and after bias correction is applied, using the melting snow as a 0 °C temperature reference, with pixels classified by temperature.

The snow surface temperature measured in each TIR image was determined by finding the coldest peak in the histogram of image pixel values from within the center of each image (Figure 2b) binned by the TIR camera's NEΔT interval. The image centers were used to avoid vignetting effects near image edges, where temperatures were biased high by as much as 2.0 °C. For each TIR image, the bias was defined as the difference between the temperature at this peak in the original image, and the reference melting snow surface temperature of 0 °C. These biases were then subtracted from each image as a scene average correction to shift the snow temperature to 0 °C.

In situ measurements of T_{ss}, T_w, and T_f at Sagehen were compared against the bias corrected aircraft (~1.5 m resolution) and UAS (submeter resolution) TIR imagery that contained each surface of interest near the image center, to evaluate this methodology. The center of images (Figure S1) were specifically targeted to avoid any vignetting effects (see Text S1). The root-mean-square error (RMSE) between the observed surface temperatures within each TIR image and the concurrent in situ measured temperatures were calculated. Snow surface temperatures were retrieved from images (aircraft TIR images $n = 84$; UAS TIR images $n = 41$) of the large snow-covered meadow that was directly measured by the ground-based radiometer (Figure S3a) by averaging temperatures across a manually identified area of approximately 5 × 5 m in each image, within the boom-mounted radiometer's 5 × 15 m footprint ellipse. Water surface temperatures were retrieved from aircraft ($n = 84$) and UAS TIR images ($n = 25$) that presented clear views of the portion of Sagehen Creek in the study area. Four manually defined areas along the widest visible portions of the creek, each approximately 2.5 × 2.5 m, were sampled from both imagery sources, and mean water surface temperatures were calculated from the pixels within these areas. Forest canopy temperatures were retrieved from pixels within a manually defined 4.5 × 4.5 m bounding box (aircraft $n = 84$; UAS $n = 41$), defining the area of interest around the small radiometer instrumented tree (Figures 1e and 2a), and a larger nearby tree cluster (aircraft $n = 84$).

3.2. TIR Over Forests and Snow

3.2.1. Image Resolution Tests

The bias of surface temperature retrievals due to mixed pixels was investigated using TIR observations of targeted areas at multiple image resolutions. Three UAS flights captured TIR imagery over forest canopy areas at a range of image resolutions by gradually raising their flight altitude while hovering above the canopy crown. This provided image resolutions at ground elevation ranging from 3–10 cm/pixel for flight altitudes of 20–70 m AGL at Sagehen, and 7–20 cm/pixel for flight altitudes of 40–110 m AGL at Davos. Pixels within each area of interest were classified by their temperatures (Figure 2b) as either unmixed "snow" pixels (<1 °C), which were masked out, "mixed" pixels containing portions of both snow and canopy (1–10 °C), or unmixed "canopy" pixels (>10 °C). A mixed pixel fraction for each image was calculated as the fraction of all nonsnow pixels that were classified as mixed.

To test for relationships between image resolution and canopy surface temperature retrievals, a linear regression model was fit between image resolution and the mixed pixel fraction, and a second linear regression model was fit between image resolution and the mean temperature of all nonsnow pixels. To determine the significance of the relationships described by these linear regressions, Monte Carlo tests were used to perturb the temperature values of each image by introducing a normally distributed error within ±1 °C (larger than the random noise that would be expected for these TIR imagers) and recomputing the regressions.

Simulated forest scenes with different forest stand configurations and fractional vegetated areas (f_{veg}), were generated and upscaled (pixel aggregation) to replicate the effect of decreasing image resolution. To represent true surface temperatures of forest canopy and snow surfaces across a 400 m^2 area at 1 cm resolution, an array of 2,000 × 2,000 pixels was created for each simulated scene. Forests were created in two different two-dimensional forest stand configurations against a snow background: a single circular dense tree cluster at the center of the scene, and a grid of 2 m diameter circular tree canopies spaced at a uniform interval to represent a sparse forest. All snow pixels were set to 0 °C and canopy pixels set to 15 °C. Each pair of simulated scenes was created with the same f_{veg}, where the diameter of the cluster in the dense forest and the spacing between the tree canopies in the sparse configuration were varied to test the impacts at a range of f_{veg} values within 0.1–0.8.

To simulate retrieving TIR images of these forest scenes at coarser resolutions, we used a 5 × 5 Gaussian kernel to approximate a TIR imager point spread function (Cracknell, 1998; Garnier et al., 1999). The point spread function encapsulates pixel response to incident radiation given the optical and electrical constraints of the TIR imager, including pixel overlap effects (Calle et al., 2009). Scenes of both forest configurations were then upscaled through repeated convolutions with this kernel from their original 1 cm resolution until the entire simulated scene was contained within one 20 m pixel. A range of f_{veg} values (0.1–0.8) for each forest configuration were tested, and temperature statistics for each upscaled scene were then compared against their original simulated "ground truth" values.

3.2.2. View Angle Tests

We investigated how off-nadir view angles over forests and snow bias surface temperature measurements by looking across the 40° × 30° field of view of the aircraft-mounted TIR camera in images of a ~1 km^2 area at Sagehen. This provided us with view angles of up to 25° off-nadir at the image corners. In this analysis, variations in forest density and temperature across the study site are not considered, but would be expected to influence patterns between retrieved surface temperatures and view angle at sites with more rugged terrain, steeper elevation gradients, and varying forest densities.

At off-nadir view angles, the use of f_{veg} to describe the linear mixing of forest canopy and snow surface temperatures needs to be substituted for a different measure that accounts for the view geometry over the complex forest canopy surface. Viewable gap fraction (VGF) describes the portion of the ground surface visible between forest canopies at a specific view angle and has been used in the analyses of the view angle effect on visible and shortwave IR observations of fractional snow-covered area (Liu & Weng, 2008; Nolin, 2011; Xin et al., 2012).

Temperature statistics (mean, standard deviation) were computed for concentric 1° view angle bands moving outward from the center of each image (near nadir). The fractional area composed of snow pixels (classified as pixels <1 °C), used as a measure of the VGF, was also calculated for each 1° view angle band. Linear least-squares regressions were used to fit VGF and the temperature summary statistics across all images with view angle to test for view angle effects on the observed surface temperatures.

The influence of sunlight and shading on retrieving forest canopy temperatures at off-nadir view angles was also investigated by computing the mean canopy surface temperature (for pixels >1 °C) within 1° azimuth bins from the same image collection ($n = 84$ images). Azimuth angles were calculated as the direction from which the camera was viewing (e.g., camera views toward the north were defined as azimuth angles viewing the forest canopy from the south).

To test the ability of these airborne TIR measurements to retrieve snow surface temperature within the viewable gap fraction, small forest gaps were manually identified around the Sagehen site. Pixel temperatures from the aircraft's 1.5 m resolution TIR imagery ($n = 84$ images) were retrieved from the center pixels within each gap to compare against in situ snow surface temperature measurements.

Table 2
Surface Temperature Retrieval Biases Before and After Bias Correction

TIR system	Bias range and σ (°C)	Surface	RMSE (°C) Before	RMSE (°C) After
DRS UC640-17 with KT15.85D	0.7–2.2 σ = 0.4	T_{ss}	1.5	0.2
		T_w	2.4	1.7
		T_f	10.3	11.7
		T_f*	3.4	3.0
ICI 8640P	−2.9–3.0 σ = 1.0	T_{ss}	2.0	0.7
		T_w	2.1	1.0
		T_f	3.3	2.3

Note. Root-mean-square errors of retrieved surface temperatures of snow (T_{ss}), water (T_w), and forest canopy (T_f) before and after bias correction (*denotes canopy temperature retrieval from a larger tree cluster that was better resolved at ~1.5 m image resolution).

4. Results

4.1. TIR Calibration Results

The use of melting snow surface temperature (T_{ss} = 0 °C) as a calibration reference for instrument bias correction (section 3.1) was validated against in situ measurements of snow, water, and tree canopy temperatures at Sagehen. These results are summarized as the range and standard deviation of biases encountered across all uncorrected images, and the RMSEs before and after bias correction in Table 2.

The UAS TIR system had a larger range of nonnormally distributed surface temperature retrieval biases (Figure S6a) and greater baseline RMSE over snow than the aircraft TIR system (Table 2). This nonnormal distribution of biases suggests a systematic rather than random source of error, which prior work has identified as likely incident sunlight on the camera body, ambient air temperature, or heating from electrical components (Dugdale et al., 2019). Biases in the aircraft TIR images matched a normal distribution more closely (Figure S6b), suggesting that these are residual errors left over after calibration with the airborne TIR system's KT radiometer. However, the aircraft was unable to clearly resolve the temperature of the small, instrumented tree canopy (Figure 1e), reflected by greater RMSE both before and after the bias correction was applied. Issues related to image resolution are discussed further in section 4.2. The bias correction using the melting snow surface as a reference decreased RMSE by about 1.0 °C in all other cases (Table 2).

There were no identifiable patterns in bias as a function of time since the shutter closed in the UAS system, suggesting that biases are not a function of linear drift, but instead are controlled by external factors that affect the TIR camera body temperature, such as ambient air temperature or incident sunlight on the camera body. Our results also suggest that periodic calibrations (i.e., internal shutter) are not as effective as having a reference temperature present in each scene, an advantage of performing TIR observations over sites containing melting snow.

4.2. TIR Over Forests and Snow Results

4.2.1. Effects of Image Resolution and Forest Structure

We tested the effects of image resolution and forest structure (sparse vs. clumped) on the sensor's ability to retrieve actual T_{ss} and T_f using observations from our field sites and simulated data (Figure 3). In the case of the single tree surrounded by open snow at Sagehen (Figures 1e and 3a), the fraction of canopy contained within mixed pixels increased by 20% as image resolutions decreased from 3 to 10 cm (Figure S7a). As the pixels containing canopy mixed more with the adjacent snow surfaces with decreasing resolutions, the mean retrieved T_f decreased by more than 3 °C (Figure S7b). For the two tree clusters at Davos, where image resolutions decreased from 7 to 20 cm, there were less significant changes in mixed pixel fractions and mean retrieved T_f. The mixed pixel fraction increased by less than 5%, and there was no statistically significant change in retrieved mean T_f at the tree cluster in the more densely forested area (Figure 3b). The tree cluster surrounded by open snow (Figure 3c) saw an increase of mixed pixels by 10% and decrease in mean retrieved T_f of 2 °C.

Mixed pixels dominated the simulated sparse forest scenes when f_{veg} was <0.7. With these low f_{veg} values, individual 2 m diameter tree canopies could not be resolved without pixels mixing with the surrounding snow surface. Only at $f_{veg} > 0.7$, when the small tree canopies were close together, could the simulated observations retrieve unmixed canopy temperatures. Conversely, unmixed snow surface temperatures could only be retrieved with $f_{veg} < 0.25$ with this sparse forest configuration. As an illustrative example (Figure 3d), when observed at a resolution of ~1.5 m, the simulated sparse forest scene with $f_{veg} = 0.13$ shows all trees contained within mixed pixels, whereas T_{ss} can be retrieved from unmixed snow-only pixels. This figure resembles the aircraft TIR observations of the isolated tree canopy at Sagehen (Figure 3a), which resulted in a large T_f RMSE (11.7 °C) as the canopy blurred with the surrounding snow surface. The retrieved surface temperature distribution over a sparse forest with significant pixel mixing will not reflect the true surface temperature variability (Figure S8a). In contrast to sparse forests, the simulated

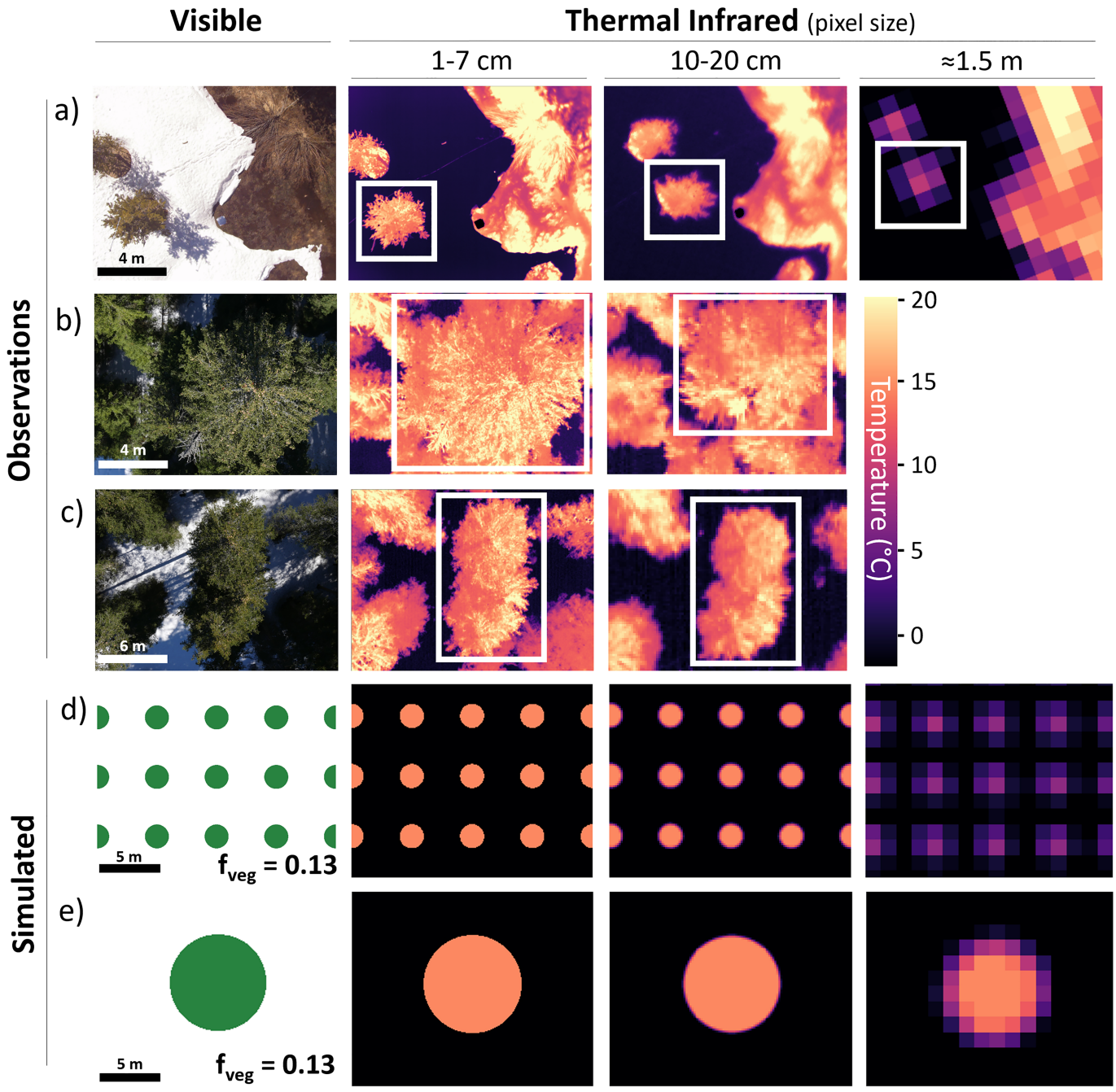

Figure 3. Observing forest canopy temperatures against snow surfaces at a range of image resolutions over (a) a single small tree canopy at Sagehen, (b) a tree cluster in a densely forested area at Davos, and (c) a tree cluster in a more sparsely forested area at Davos. Simulated (d) sparse forest and (e) a dense tree cluster were generated to investigate the influence of forest distribution and f_{veg} on surface temperature retrievals at coarser resolutions. (Scale bars estimated from ground sample distance computed for each image.)

observations of a dense tree cluster could retrieve T_f from unmixed pixels at a wide range of f_{veg} values. Also illustrated with an f_{veg} = 0.13 in Figure 3e, this dense forest cluster had only 42% of its canopy contained within mixed pixels at ~1.5 m resolution, and the true canopy temperature could be retrieved from pixels at the center of the cluster, away from its edges. Surface temperatures retrieved from a forest structured with dense tree clusters like this could result in a distribution closer to that of the true temperature variability (Figure S8b), which could be used to identify the two end-members (trees and snow), as the warmest and coldest points, respectively, within the scene.

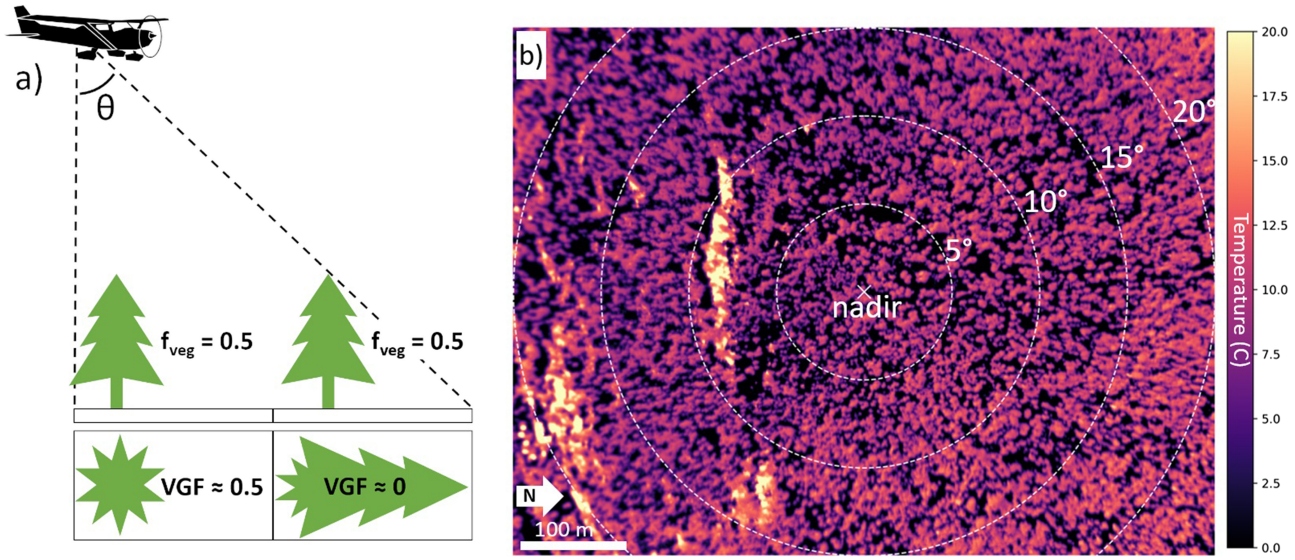

Figure 4. (a) Illustration of the effect of off-nadir view angles over forests and snow, where forest gaps are obscured (and the VGF reduced) by trees near the edges of the image field of view (θ) even with a nearly constant f_{veg} (adapted from Liu & Weng, 2008). (b) This reduction in VGF is seen in the aircraft-based TIR images over Sagehen near the image edges where view angles are the furthest off-nadir (θ > 20°).

4.2.2. Effects of Off-Nadir View Angles

As off-nadir view angles increased (Figure 4), the mean VGF at Sagehen decreased at a rate of about 0.9% per degree (from about 30% at nadir to 5% at 25° off-nadir; Figure S9a). The mean pixel temperature increased with increasing off-nadir view angles, at a rate of 0.07 °C per degree (Figure S9b). This translated to higher apparent temperatures (+1.75 °C) at image edges than at the center, as snow in forest gaps was obscured by the warmer forest canopy. The standard deviation of measured surface temperatures decreased by 1.1 °C as view angles increased and mean temperatures converged toward canopy temperatures (Figure S9c). Views toward the northeast (viewing the southwest portion of canopies) retrieved mean canopy temperatures about 2 °C warmer than views toward the south (north facing portion of canopies) (Figure S10), demonstrating a retrieved temperature dependence on solar illumination angle (solar azimuth angle of ~220° at the time of observation) as well as camera view angle. With TIR observations at 1.5 m resolution, the snow surface temperatures retrieved from within visible forest gaps were most accurate for visible gaps larger than 10 m in diameter. TIR observations of snow surface temperature were biased higher, approaching the temperature of the surrounding forest canopy, within smaller gaps (Figure S11), as more of the retrieved pixels were mixed.

5. Discussion and Applications

5.1. Melting Snow as a TIR Calibration Target

Using melting snow as a constant 0 °C reference for bias correction decreased surface temperature retrieval errors for uncooled TIR imagers. For features that could be resolved by the submeter resolution UAS TIR and ~1.5 m resolution aircraft TIR, surface temperature RMSEs were reduced by about 1 °C using this method. Correcting for this instrument bias is especially needed for airborne observations where periodic internal shutter recalibrations cannot compensate for the effects of ambient air temperature and incident sunlight changing the camera body temperature rapidly. This is essential when observations of absolute surface temperatures or interimage comparisons of surface temperatures are needed, rather than relative temperature differences within a single image. Images should be corrected prior to mosaicking, rather than a single correction used across an entire mosaic. This bias correction method does not need to assume any functional form of the bias, such as a linear drift with time or as a function of external air temperature and can therefore correct for the myriad of influences that cause microbolometer arrays to change temperature. However, this method was unsuccessful when tested in more densely forested regions further away from the main Sagehen

study site. In these areas the snow signal within the histogram could not be readily identified, and instead a "mixed" forest edge temperature peak was more prominent (see section 5.2).

If snow surface temperature across an area of interest exhibits spatial temperature heterogeneities (e.g., the temperature of shaded versus sunlit snow), portions identified as undergoing melt at 0 °C could be delineated and used for TIR camera bias correction. Similarly, more accurate surface temperatures could be retrieved across areas with more variable surface types if an emissivity correction is performed (Aubry-Wake et al., 2015) following the bias correction step. Without melting snow surfaces at a study site, airborne TIR observations over a small area could instead rely on thermal targets placed within the field of view of the TIR camera, so that a unique bias correction could be determined and applied for each image (Aubry-Wake et al., 2015). However, for the more common scenario of airborne TIR observations over large areas, installing multiple targets can be logistically difficult or impossible. The water surface temperature of a well-mixed stream could provide another blackbody-like thermal target (Baker et al., 2019; Dugdale et al., 2019). Alternatively, as was used on the aircraft's TIR system at Sagehen, including a higher accuracy IR radiometer alongside the TIR camera can be used for bias corrections. A radiometer sampling at a high rate allows for vicarious calibration of each individual image, rather than having to rely on the intermittent calibrations using an internal shutter common on many of these TIR cameras.

5.2. TIR Image Resolution and View Angles Over Snow and Forests

Airborne TIR observations at a range of spatial resolutions demonstrated the linear mixing of subpixel forest and snow temperatures where subpixel temperatures are within 25 K of each other (Liu et al., 2006; McCabe et al., 2008). At coarser resolutions the mean retrieved canopy temperatures at forest edges were biased lower as they became blurred with the adjacent snow surfaces. Retrieving accurate, unmixed, surface temperatures of small features, such as narrow streams like Sagehen Creek, requires an image resolution fine enough to cover the feature with at least 10 pixels (Handcock et al., 2006; Torgersen et al., 2001). This was seen in our attempts to retrieve the canopy temperature of a single small tree (Figure 3a) and snow surface temperature within forest gaps smaller than 10 m in diameter with 1.5 m pixels (Figure S11).

For satellite thermal infrared remote sensing over heterogeneous forest snow areas, with pixel sizes greater than 30 m (Selkowitz et al., 2014), we could expect to retrieve a mean, linearly mixed surface temperature in proportion to the pixel's f_{veg} at nadir, or to the VGF when off-nadir (McCabe et al., 2008). Some of these satellite sensors benefit from the inclusion of midwave IR bands (VIIRS, MODIS, GOES ABI, Himawari AHI) or 8–9 μm TIR bands (ECOSTRESS) in addition to their longer wavelength TIR bands. Using the difference in radiance observed through multiple IR bands can permit the use of spectral unmixing to retrieve subpixel surface temperatures (Dozier, 1981), such as for separating forest canopy from snow surface temperatures (Lundquist et al., 2018).

The simulated forest scenes showed that TIR remote sensing retrieves different surface temperature distributions over forest snow environments depending on the spatial distribution of forest stands, and not on f_{veg} alone. Forests with more uniform distributions of tree stands and gaps will have more forest edges susceptible to blurring with the adjacent snow background. TIR images of these sites with more mixed pixels will retrieve temperature distributions that converge toward a mean of the canopy and snow surface temperatures. Observations over forests with large tree clumps and/or wide forest gaps will have fewer mixed pixels and could retrieve temperature distributions that better represent the true distribution. An aggregate parameter to quantify forest spatial configuration, such as lidar-derived canopy gap size distributions (Mazzotti et al., 2019), could be used to describe the expected bias in observed surface temperature distribution due to the effects of mixed pixels for coarser resolution airborne or satellite-based observations.

When observed from off-nadir view angles, the forest's VGF decreased, and mean retrieved temperatures increased, as trees obscured more of the snow surface behind and beneath them. For the creation of image mosaics from such images, some allowance of acceptable off-nadir view angles would have to be determined based on local tree height, to minimize these effects. The portion of images beyond these acceptable view angles, toward the edges of the field of view, would then be trimmed away (Kelly et al., 2019). This limits the usefulness of wide field of view lenses on TIR cameras over forests.

While off-nadir view angles may hinder measurements of snow surface temperature within forests, they present an opportunity to retrieve unmixed canopy temperature pixels even with coarser resolution imagery.

Observations of forests at large view angles would allow measurements of canopy temperature regardless of ground cover and could be applied to studying seasonal mountain meteorological conditions (Essery et al., 2008), informing models of longwave radiation over snowpack (Webster et al., 2017), or monitoring forest health (Wang & Dickinson, 2012). However, observations from these view angles would also need to consider the direction of incident sunlight (Henderson et al., 2004) to determine if observations are biased due to viewing sunlit or shaded portions of the canopy (Figure S10), or to visibility of warmer tree trunks (Webster et al., 2018).

Spectral unmixing methods used to retrieve forest and snow temperatures from mixed pixels need the local VGF determined for off-nadir view angles, such as from geostationary satellite sensors (GOES ABI, Himawari AHI), or near the edges of wide swaths (MODIS, VIIRS). This VGF can be calculated through models that use independent forest structure information (Liu & Weng, 2008), or by solving directly for the fractional viewable snow covered area (equal to 1-VGF) across multiple adjacent pixels at once (Lundquist et al., 2018).

6. Conclusions

Instrument bias of uncooled TIR cameras was identified as a significant source of error, impacting the measurement of accurate surface temperatures from airborne platforms over conifer forests and snow. We applied a bias correction method using the constant 0 °C melting snow surface as a natural calibration target and demonstrated its ability to improve the accuracy of UAS and aircraft-based TIR surface temperature measurements. Without this natural calibration target, the vicarious calibration method employed by the aircraft-based TIR system demonstrated better performance than the periodic internal shutter calibrations of the UAS TIR system. The observed temperature distribution of a forest snow scene was found to depend on image resolution and the underlying forest configuration. Coarse resolution observations of sparse forests with more edges will retrieve more mixed pixels than the observations of a forest with dense tree clumps and large gaps at the same resolution. At off-nadir view angles greater than 20°, the forest canopy at Sagehen began to obscure snow in forest gaps from view, biasing the mean temperatures retrieved from image edges higher than those from image centers. These off-nadir views could allow canopy temperature measurements from airborne or satellite remote sensing platforms without the issue of including mixed pixels from the snow or ground surface below.

Acknowledgments
We gratefully acknowledge the following individuals: Clemens Hiller (SLF Davos) and Nick Rutter (Northumbria University, UK) for the UAS data acquisition at the Davos site; Rosangela Carreon, Sarah Petersen, and Jenna Weiner (UNR) for their help with fieldwork at Sagehen; Chris Kratt, Chris Sladek (UNR), and the Center for Transformative Environmental Monitoring Programs (CTEMPS) for the UAS flights at Sagehen; APL engineer Dan Clark and those at Regal Air including president Ron Morcom, engineer Bill Retzlaff, and our pilot Greg Maust for the TIR acquisition flights over Sagehen, and David Shean (UW) for providing valuable feedback on this manuscript and insight into airborne observations and UAS operations. We would also like to thank WRR Editor Martyn Clark, Associate Editor Tobias Jonas, reviewers Jeff Dozier, Oliver Wigmore, and our third anonymous reviewer, whose comments and questions helped to greatly improve this manuscript. The data used in this study can be accessed through the Mountain Hydrology Research Group collection within the University of Washington Library ResearchWorks Archive (https://digital.lib.washington.edu/researchworks/handle/1773/25604). Sample code for the snow-based TIR bias correction and analysis is available on GitHub (https://github.com/spestana/forest-snow-tir). Funding and instrumentation support was provided by NASA Grants NNX15AB29G, NNX17AL59G, and NNX14AN24A, and National Science Foundation Grant EAR-1440596.

References

Abolt, C., Caldwell, T., Wolaver, B., & Pai, H. (2018). Unmanned aerial vehicle-based monitoring of groundwater inputs to surface waters using an economical thermal infrared camera. *Optical Engineering*, *57*(05), 1. https://doi.org/10.1117/1.OE.57.5.053113

Aubry-Wake, C., Baraer, M., McKenzie, J. M., Mark, B. G., Wigmore, O., Hellström, R. Å., et al. (2015). Measuring glacier surface temperatures with ground-based thermal infrared imaging. *Geophysical Research Letters*, *42*, 8489–8497. https://doi.org/10.1002/2015GL065321

Baker, E. A., Lautz, L. K., McKenzie, J. M., & Aubry-Wake, C. (2019). Improving the accuracy of time-lapse thermal infrared imaging for hydrologic applications. *Journal of Hydrology*, *571*, 60–70. https://doi.org/10.1016/j.jhydrol.2019.01.053

Budzier, H., Gerlach, G., 2011. (Translated by Müller, D.,), *Thermal infrared sensors: Theory, optimization, and practice*. John Wiley & Sons, Ltd, Chichester, UK. https://doi.org/10.1002/9780470976913

Calle, A., Casanova, J. L., & González-Alonso, F. (2009). Impact of point spread function of MSG-SEVIRI on active fire detection. *International Journal of Remote Sensing*, *30*(17), 4567–4579. https://doi.org/10.1080/01431160802609726

Cracknell, A. P. (1998). Review article Synergy in remote sensing-what's in a pixel? *International Journal of Remote Sensing*, *19*(11), 2025–2047. https://doi.org/10.1080/014311698214848

Cristea, N. C., & Burges, S. J. (2009). Use of thermal infrared imagery to complement monitoring and modeling of spatial stream temperatures. *Journal of Hydrologic Engineering*, *14*(10), 1080–1090. https://doi.org/10.1061/(asce)he.1943-5584.0000072

Dozier, J. (1981). A method for satellite identification of surface temperature fields of subpixel resolution. *Remote Sensing of Environment*, *11*, 221–229. https://doi.org/10.1016/0034-4257(81)90021-3

Dozier, J., & Warren, S. G. (1982). Effect of viewing angle on the infrared brightness temperature of snow. *Water Resources Research*, *18*(5), 1424–1434. https://doi.org/10.1029/WR018i005p01424

Dugdale, S. J., Kelleher, C. A., Malcolm, I. A., Caldwell, S., & Hannah, D. M. (2019). Assessing the potential of drone-based thermal infrared imagery for quantifying river temperature heterogeneity. *Hydrological Processes*, *33*(7), 1152–1163. https://doi.org/10.1002/hyp.13395

Essery, R., Bunting, P., Rowlands, A., Rutter, N., Hardy, J., Melloh, R., et al. (2008). Radiative transfer modeling of a coniferous canopy characterized by airborne remote sensing. *Journal of Hydrometeorology*, *9*(2), 228–241. https://doi.org/10.1175/2007JHM870.1

Garnier, C., Collorec, R., Flifla, J., Mouclier, C., & Rousee, F. (1999). Infrared sensor modeling for realistic thermal image synthesis. In *1999 IEEE International Conference on Acoustics, Speech, and Signal Processing. Proceedings. ICASSP99 (Cat. No. 99CH36258)* (Vol. 6, pp. 3513–3516). IEEE. https://doi.org/10.1109/icassp.1999.757600

Gómez-Candón, D., Virlet, N., Labbé, S., Jolivot, A., & Regnard, J. L. (2016). Field phenotyping of water stress at tree scale by UAV-sensed imagery: New insights for thermal acquisition and calibration. *Precision Agriculture*, *17*(6), 786–800. https://doi.org/10.1007/s11119-016-9449-6

Handcock, R. N., Gillespie, A. R., Cherkauer, K. A., Kay, J. E., Burges, S. J., & Kampf, S. K. (2006). Accuracy and uncertainty of thermal-infrared remote sensing of stream temperatures at multiple spatial scales. *Remote Sensing of Environment*, *100*(4), 427–440. https://doi.org/10.1016/j.rse.2005.07.007

Harvey, M. C., Rowland, J. V., & Luketina, K. M. (2016). Drone with thermal infrared camera provides high resolution georeferenced imagery of the Waikite geothermal area, New Zealand. *Journal of Volcanology and Geothermal Research*, *325*(June), 61–69. https://doi.org/10.1016/j.jvolgeores.2016.06.014

Henderson, B. G., Balick, L. K., Rodger, A. P., & Pope, P. A. (2004). Concurrent measurements of directional reflectance and temperature of a wintertime coniferous forest from space. *Ecosystems' Dynamics, Agricultural Remote Sensing and Modeling, and Site-Specific Agriculture*, *5153*(December 2003), 21. https://doi.org/10.1117/12.506296

Howard, R., & Stull, R. (2013). IR radiation from trees to a ski run: A case study. *Journal of Applied Meteorology and Climatology*, *52*(7), 1525–1539. https://doi.org/10.1175/JAMC-D-12-0222.1

Jensen, A. M., McKee, M., & Chen, Y. Q. (2014). Procedures for processing thermal images using low-cost microbolometer cameras for small unmanned aerial systems. *IEEE Geoscience and Remote Sensing Symposium*, *2014*, 2629–2632. https://doi.org/10.1109/IGARSS.2014.6947013

Kelly, J., Kljun, N., Olsson, P.-O., Mihai, L., Liljeblad, B., Weslien, P., et al. (2019). Challenges and best practices for deriving temperature data from an uncalibrated UAV thermal infrared camera. *Remote Sensing*, *11*, 567. https://doi.org/10.3390/rs11050567

Kraaijenbrink, P. D. A., Shea, J. M., Litt, M., Steiner, J. F., Treichler, D., Koch, I., & Immerzeel, W. W. (2018). Mapping surface temperatures on a debris-covered glacier with an unmanned aerial vehicle. *Frontiers in Earth Science*, *6*, 64. https://doi.org/10.3389/feart.2018.00064

Lapo, K. E., Hinkelman, L. M., Raleigh, M. S., & Lundquist, J. D. (2015). Impact of errors in the downwelling irradiances on simulations of snow water equivalent, snow surface temperature, and the snow energy balance. *Water Resources Research*, *51*, 1649–1670. https://doi.org/10.1002/2014WR016259

Liu, H., & Weng, Q. (2008). Seasonal variations in the relationship between landscape pattern and land surface temperature in Indianapolis, USA. *Environmental Monitoring and Assessment*, *144*(1-3), 199–219. https://doi.org/10.1007/s10661-007-9979-5

Liu, Y., Hiyama, T., & Yamaguchi, Y. (2006). Scaling of land surface temperature using satellite data: A case examination on ASTER and MODIS products over a heterogeneous terrain area. *Remote Sensing of Environment*, *105*(2), 115–128. https://doi.org/10.1016/j.rse.2006.06.012

Lundquist, J. D., & Cayan, D. R. (2007). Surface temperature patterns in complex terrain: Daily variations and long-term change in the central Sierra Nevada, California. *Journal of Geophysical Research*, *112*, D11124. https://doi.org/10.1029/2006JD007561

Lundquist, J. D., Chickadel, C., Cristea, N., Currier, W. R., Henn, B., Keenan, E., & Dozier, J. (2018). Separating snow and forest temperatures with thermal infrared remote sensing. *Remote Sensing of Environment*, *209*, 764–779. https://doi.org/10.1016/j.rse.2018.03.001

Mazzotti, G., Currier, W. R., Deems, J. S., Pflug, J. M., Lundquist, J. D., & Jonas, T. (2019). Revisiting snow cover variability and canopy structure within forest stands: Insights From airborne lidar data. *Water Resources Research*, *55*, 6198–6216. https://doi.org/10.1029/2019WR024898

McCabe, M. F., Balick, L. K., Theiler, J., Gillespie, A. R., & Mushkin, A. (2008). Linear mixing in thermal infrared temperature retrieval. *International Journal of Remote Sensing*, *29*(17-18), 5047–5061. https://doi.org/10.1080/01431160802036474

Mesas-Carrascosa, F. J., Pérez-Porras, F., de Larriva, J. E. M., Frau, C. M., Agüera-Vega, F., Carvajal-Ramírez, F., et al. (2018). Drift correction of lightweight microbolometer thermal sensors on-board unmanned aerial vehicles. *Remote Sensing*, *10*(4), 1, 615–18. https://doi.org/10.3390/rs10040615

Nolin, A. W. (2011). Recent advances in remote sensing of seasonal snow. *Journal of Glaciology*, *56*(200), 1141–1150. https://doi.org/10.3189/002214311796406077

Norman, J. M., & Becker, F. (1995). Terminology in thermal infrared remote sensing of natural surfaces. *Agricultural and Forest Meteorology*, *77*(3-4), 153–166. https://doi.org/10.1016/0168-1923(95)02259-Z

Nugent, P. W., Shaw, J. A., & Pust, N. J. (2013). Correcting for focal-plane-array temperature dependence in microbolometer infrared cameras lacking thermal stabilization. *Optical Engineering*, *52*(6), 061304. https://doi.org/10.1117/1.OE.52.6.061304

Pai, H., Burnett, J., Sladek, C., Wing, M., Feigl, K., Selker, J., Tyler, S., & PoroTomo Team (2016). Analyzing the potential for Unmanned Aerial Systems (UAS) photogrammetry in estimating surface deformations at a geothermal field. In AGU Fall Meeting Abstracts.

Pai, H., Malenda, H. F., Briggs, M. A., Singha, K., González-Pinzón, R., Gooseff, M. N., & Tyler, S. W. (2017). Potential for small unmanned aircraft systems applications for identifying groundwater-surface water exchange in a meandering river reach. *Geophysical Research Letters*, *44*, 11,868–11,877. https://doi.org/10.1002/2017GL075836

Ribeiro-Gomes, K., Hernández-López, D., Ortega, J. F., Ballesteros, R., Poblete, T., & Moreno, M. A. (2017). Uncooled thermal camera calibration and optimization of the photogrammetry process for UAV applications in agriculture. *Sensors (Switzerland)*, *17*(10), 9–11. https://doi.org/10.3390/s17102173

Salisbury, J. W., & D'Aria, D. M. (1992). Emissivity of terrestrial materials in the 8–14 μm atmospheric window. *Remote Sensing of Environment*, *42*(2), 83–106. https://doi.org/10.1016/0034-4257(92)90092-X

Selkowitz, D. J., Forster, R. R., & Caldwell, M. K. (2014). Prevalence of pure versus mixed snow cover pixels across spatial resolutions in alpine environments. *Remote Sensing*, *6*, 12478–12508. https://doi.org/10.3390/rs61212478

Shea, C., & Jamieson, B. (2011). Some fundamentals of handheld snow surface thermography. *The Cryosphere*, *5*(1), 55–66. https://doi.org/10.5194/tc-5-55-2011

Sheng, H., Chao, H., Coopmans, C., Han, J., McKee, M., & Chen, Y. Q. (2010). Low-cost UAV-based thermal infrared remote sensing: Platform, calibration and applications. *Proceedings of 2010 IEEE/ASME International Conference on Mechatronic and Embedded Systems and Applications, MESA 2010*, 38-43. https://doi.org/10.1109/MESA.2010.5552031

Torgersen, C. E., Faux, R. N., McIntosh, B. A., Poage, N. J., & Norton, D. J. (2001). Airborne thermal remote sensing for water temperature assessment in rivers and streams. *Remote Sensing of Environment*, *76*(3), 386–398. https://doi.org/10.1016/S0034-4257(01)00186-9

U.S. Geological Survey (USGS), (2016). National Water Information System data available on the world wide web (USGS Water Data for the Nation), accessed August 2018, at URL https://waterdata.usgs.gov/nwis/inventory?agency_code = USGS&site_no = 10343500 https://doi.org/10.5066/F7P55KJN

Wang, K., & Dickinson, R. E. (2012). A review of global terrestrial evapotranspiration: bservation, modelling, climatology, and climatic variability. *Reviews of Geophysics*, *50*, RG2005. https://doi.org/10.1029/2011RG000373

Warren, S. G. (1982). Optical properties of snow. *Reviews of Geophysics*. https://doi.org/10.1029/RG020i001p00067

Webster, C., Rutter, N., & Jonas, T. (2017). Improving representation of canopy temperatures for modeling subcanopy incoming longwave radiation to the snow surface. *Journal of Geophysical Research: Atmospheres*, *122*, 9154–9172. https://doi.org/10.1002/2017JD026581

Webster, C., Westoby, M., Rutter, N., & Jonas, T. (2018). Three-dimensional thermal characterization of forest canopies using UAV photogrammetry. *Remote Sensing of Environment*, *209*, 835–847. https://doi.org/10.1016/j.rse.2017.09.033

Whiteman, C. D. (2004). Comparison of vertical soundings and sidewall air temperature measurements in a small alpine basin. *Journal of Applied Meteorology*, *43*(11), 1635–1647.

Wigmore, O., Mark, B., McKenzie, J., Baraer, M., & Lautz, L. (2019). Sub-metre mapping of surface soil moisture in proglacial valleys of the tropical Andes using a multispectral unmanned aerial vehicle. *Remote Sensing of Environment*, *222*, 104–118. https://doi.org/10.1016/j.rse.2018.12.024

Xin, Q., Woodcock, C. E., Liu, J., Tan, B., Melloh, R. A., & Davis, R. E. (2012). View angle effects on MODIS snow mapping in forests. *Remote Sensing of Environment*, *118*(10), 50–59. https://doi.org/10.1016/j.rse.2011.10.029

Yang, G., Weng, Q., Pu, R., Gao, F., Sun, C., Li, H., & Zhao, C. (2016). Evaluation of ASTER-like daily land surface temperature by fusing ASTER and MODIS data during the HiWATER-MUSOEXE. *Remote Sensing*. https://doi.org/10.3390/rs8010075

Reference From the Supporting Information

Meerdink, S. K., Hook, S. J., Roberts, D. A., & Abbott, E. A. (2019). The ECOSTRESS spectral library version 1.0. *Remote Sensing of Environment*, *230*, 111196. https://doi.org/10.1016/j.rse.2019.05.015